JACS
JOURNAL OF THE AMERICAN CHEMICAL SOCIETY
Article
pubs.acs.org/JACS

Electrochemistry and Electrogenerated Chemiluminescence of 1,3,5-Tri(anthracen-10-yl)-benzene-Centered Starburst Oligofluorenes

Honglan Qi,[†,‡] Chengxiao Zhang,[‡] Zhi Huang,[§] Lei Wang,[*,§] Weina Wang,[‡] and Allen J. Bard[*,†]

[†]Center for Electrochemistry, Department of Chemistry and Biochemistry, The University of Texas, Austin, Texas 78712, United States

[‡]Key Laboratory of Analytical Chemistry for Life Science of Shaanxi Province, School of Chemistry and Chemical Engineering, Shaanxi Normal University, Xi'an 710062, PR China

[§]Wuhan National Laboratory for Optoelectronics, Huazhong University of Science and Technology, Wuhan 430074, PR China

Supporting Information

ABSTRACT: The electrochemistry and electrogenerated chemiluminescence (ECL) of three 1,3,5-tri(anthracen-10-yl)-benzene-centered starburst oligofluorenes (T1−T3) are reported in this paper. The compounds T1−T3 contain 1,3,5-tri(anthracen-10-yl)-benzene as a core with fluorene as an arm from monofluorene to trifluorene groups (n = 1−3), generating a rigid three-dimensional structure. The electrochemical behaviors of these compounds are likely to be tuned by the fluorene arms. In cyclic voltammograms, both the oxidation and reduction of T1 and T2 are characterized by three reversible one-electron transfers from the core while the oxidation and reduction of T3 are characterized by six reversible one-electron transfers from the core and the arms in acetonitrile:benzene (v:v = 1:1) solvent. The second oxidation and reduction waves of T1 show three reversible one-electron transfers from three fluorene arms, while the second and third oxidation and reduction waves of T2 and T3 exhibit three reversible one-electron transfers from the six fluorene arms. The multiple electron transfers in one molecule are confirmed by chronoamperometry at an ultramicroelectrode, simulations and DFT calculations. The T1−T3 compounds display strong absorption in UV−vis and blue fluorescence emission. Strong blue ECL emissions can be generated from T1, T2 and T3 under ion annihilation condition, which is assigned as S-route.

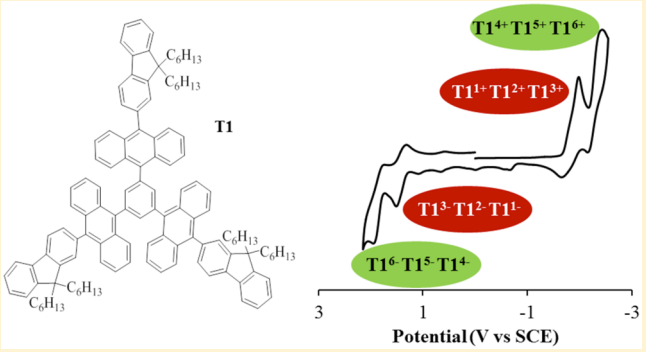

INTRODUCTION

Research on multiple electron transfers in a molecule that contains two or more identical or similar electroactive groups has been of interest in the electrochemistry of organic compounds.[1] The study of the electrochemical parameters, including potential, stability, and the energy separation between different states is fundamental research to understand the interaction between redox groups and the kinetics of these processes. A molecule that contains identical electroactive groups will only show single voltammetric wave, if the groups do not interact, such as ferrocene, other transition-metal units,[2] or redox organic groups in polymer or dendrimers.[3] If the electroactive groups interact strongly, two separate voltammetric waves at least will be observed in the potential window of the solvent/electrolyte. Generally, the addition or removal of more than two electrons is also detected in some compounds, although it is more difficult to be observed than that of the first or second electron. For instance, four or more separated voltammetric waves were observed for heptanuclear complexes,[4−6] and six successive reduction waves were observed for C60 and C70.[7] Our previous work has shown that poly(fluorene methylene) oligomers exhibit successive four one-electron oxidation waves.[8]

Star-shaped conjugated oligomers, which are usually defined as branched molecules consisting of a central core with linear polymer arms, have received attention in recent years,[9,10] since they have advantages from both the core and linear polymer arms in electrical, optical, and morphological properties.[11] These type oligomers with different cores and arms had been synthesized, and their optical, electrochemical and thermal properties had been demonstrated, such as truxene core,[12−14] spirofluorene core,[15] benzene core,[16] silsesquioxane core,[17] triazatruxene core,[18] triphenylamine core,[19] or phosphine oxide core[20] with oligofluorenes arms; a hexakis(fluoren-2-yl)benzene core with diphenylamine arms;[21] a bimesityl core with anthracene arms;[22] an isotruxene core and α-oligothiophene arms;[23] a porphyrins core with four oligofluorene arms;[24] 1,3,5-triazine cored oligomers core with three fluorene arms;[25] a triarylamines core with a 3,4-ethylenedioxythiophene linker;[26] and spirobifluorene-linked bisanthracene.[27] The optoelectronic,

Received: November 20, 2015
Published: January 21, 2016

DOI: 10.1021/jacs.5b12184
J. Am. Chem. Soc. 2016, 138, 1947−1954

electrochemical and thermal properties of the compounds mentioned above can be tuned by changing core or arm.[28] Among them, the π-conjugated oligofluorenes have received great attention due to their blue electroluminescent properties. We previously reported the synthesis and organic light-emitting diodes (OLED) properties of three compounds T1, T2 and T3, as schemed in Scheme 1.[29] The compounds T1−T3 contain

Scheme 1. Structure of T1 to T3

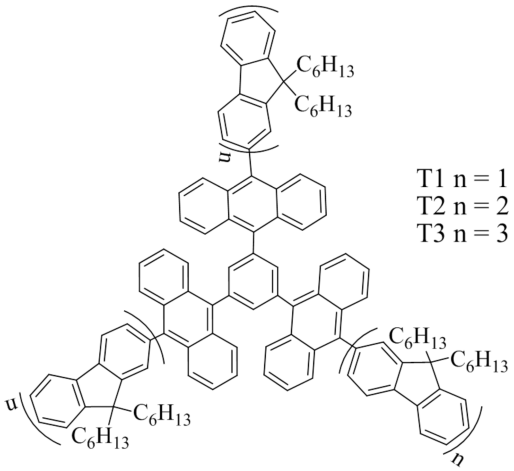

1,3,5-tri(anthracen-10-yl)-benzene as core with fluorene as arm from monofluorene to trifluorene groups (n = 1−3), possessing a propeller twist topology between the core and star. Their strongly deep blue emissions and deep-blue species for OLEDs have been demonstrated.[29] However, the electrochemistry of these compounds and electrogenerated chemiluminescence (ECL) in solution has not been reported.

We present here the electrochemistry and ECL of these three compounds in acetonitrile:benzene solution. The formal potentials of the sequential removal or addition of electrons from the core and the arms are evaluated. The mechanisms of multiple electron transfer, and the ECL in solution by ion annihilation for these three compounds are extensively investigated to understand the structure−property relationships of T1−T3.

EXPERIMENTAL SECTION

The synthesis of T1, T2 and T3 was performed as described previously.[29] The chemicals including solvents (benzonitrile, Bz, 99% and acetonitrile, MeCN, 99.8%), electrolytes (tetra-*n*-butylammonium hexafluorophosphate, $TBAPF_6$) were used as the same in our previous work.[30] The apparatus and general techniques for UV−vis absorbance, fluorescence, electrochemical and ECL measurements are the same as that reported previously.[30] Annihilation ECL spectra were recorded using an Acton SpectPro-150 monochromator with a Princeton Instruments Spec 10 CCD camera (Trenton, NJ).

All electrochemical and ECL experiments were performed in an argon atmosphere glovebox under anhydrous conditions. Three-electrode system consisted of platinum working electrode (A = 0.034 cm^2) or a gold ultramicroelectrode (UME, 10 μm radius), a platinum counter electrode and an Ag quasi-reference electrode. Ferrocene was used as an internal standard to calibrate the potentials CV, taking its formal potential as 0.342 V vs SCE.[35] The CVs were simulated using DigiSim 3.03 (Bioanalytical Systems, Inc., West Lafayette, IN). Molecular orbitals were calculated using the B3LYP functional with 6-31G(d) basis set in Gaussian 09 and visualized using GaussView software.

RESULTS AND DISCUSSION

Electrochemistry. Electrochemical experiments of T1, T2 and T3 were performed in MeCN:Bz (v:v = 1:1) solution containing 0.1 M $TBAPF_6$. Cyclic voltammograms (CVs) of T1, T2 and T3 in Figure 1 display single reversible redox waves

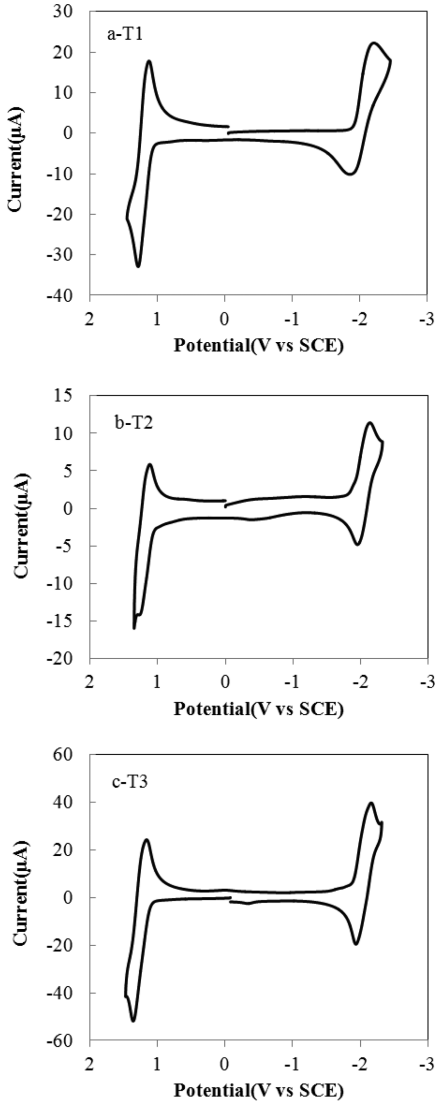

Figure 1. CVs of T1 (0.7 mM), T2 (0.4 mM) and T3 (0.7 mM) in MeCN:Bz (v:v = 1:1) solution containing 0.1 M $TBAPF_6$ at a platinum electrode (A = 0.034 cm^2). Scan rate was 0.5 V/s.

for oxidation at about +1.2 V vs SCE and reduction at about −2.1 V vs SCE. A detailed discussion about the electrochemical behaviors is presented in the following sections.

T1. Representative CV of T1 in Figure 1a clearly shows overall single waves for oxidation at 1.20 V vs SCE and reduction at −2.20 V. The CVs in different scan rates show that the peak currents are directly proportional to the square root of the scan rates (see Figure S1 in the Supporting Information). This indicates that the diffusion processes control both the reduction and oxidation currents. Furthermore, the peak current ratio for the oxidation and reduction waves of T1 is approximately unity in the range from 0.05 to 2 V/s. This indicates that the radical cation and anion generated electrochemically are highly stable.

DOI: 10.1021/jacs.5b12184
J. Am. Chem. Soc. 2016, 138, 1947−1954

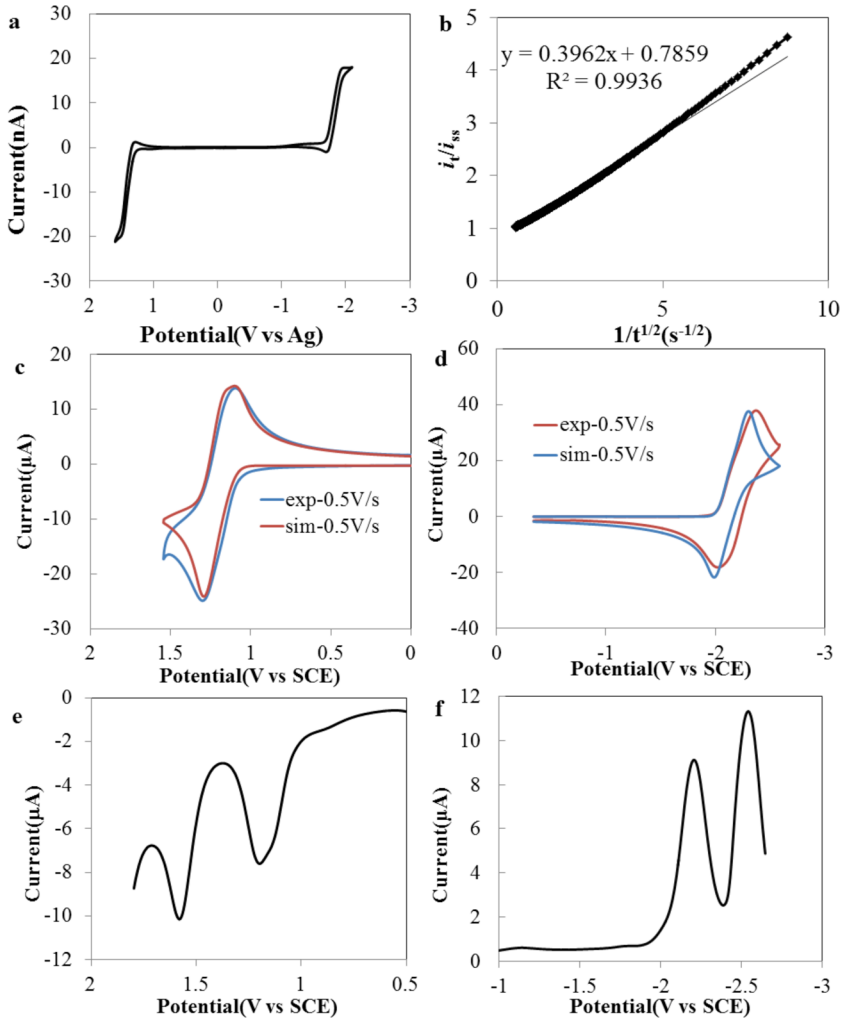

Figure 2. (a) CV of 1.1 mM T1 at gold UME (r = 10 μm), Scan rate: 10 mV/s. (b) Plot of i_t/i_{ss} vs $t^{-1/2}$ for 1.1 mM T1 at gold UME. (c) Experimental and simulated oxidation waves for 0.7 mM T1 at platinum electrode (EEE, k_1^0, k_2^0, and k_3^0 > 0.01 cm/s, $E^0_{1,ox}$ = 1.14 V, $E^0_{2,ox}$ = 1.18 V, $E^0_{3,ox}$ = 1.22 V; Diffusion coefficient: 6×10^{-6} cm^2/s, uncompensated resistance 1400 Ω, capacitance 6×10^{-7} F). (d) Experimental and simulated reduction waves for 1.1 mM T1 at platinum electrode (EEEC, k_1^0 = 0.01 cm/s, k_2^0 = 0.005 cm/s, k_3^0 = 0.005 cm/s, k_f = 1 s^{-1}; $E^0_{1,red}$ = −2.10 V, $E^0_{2,red}$ = −2.16 V, $E^0_{3,red}$ = −2.22 V; Diffusion coefficient: 6×10^{-6} cm^2/s, uncompensated resistance 1400 Ω, capacitance 1×10^{-7} F). (e) SWV of 0.7 mM T1 for oxidation; (f) SWV of 1.1 mM T1 for reduction. Experimental conditions: MeCN: Bz (v:v = 1:1) solution containing 0.1 M $TBAPF_6$.

Table 1. Redox Potentials of T1, T2, and T3 Obtained by Digital Simulation

	E^0_{ox}(V vs SCE)						E^0_{Red}(V vs SCE)					
compound mechanism	$E^0_{1,ox}$	$E^0_{2,ox}$	$E^0_{3,ox}$	$E^0_{4,ox}$	$E^0_{5,ox}$	$E^0_{6,ox}$	$E^0_{1,red}$	$E^0_{2,red}$	$E^0_{3,red}$	$E^0_{4,red}$	$E^0_{5,red}$	$E^0_{6,red}$
T1 three steps	1.14	1.18	1.22				−2.10	−2.16	−2.22			
T2 three steps	1.11	1.16	1.18				−1.98	−2.03	−2.08			
T3 six steps	1.16	1.20	1.24	1.26	1.30	1.32	−2.05	−2.09	−2.13	−2.17	−2.21	−2.25

In Figure 2a showing the CVs of T1 at a gold UME, one reduction wave and one oxidation wave were observed. This is consistent with the CV results at a macroelectrode (Figure 1a). The number of electrons involved in a single wave and the diffusion coefficient were determined by chronoamperometry at a gold UME.[31] Figure 2b shows a plot of the oxidation current ratio (i_t/i_{ss}) vs the inverse square root of time ($t^{-1/2}$) for T1 at a gold UME. From the data, the number of electrons was 3.03 and the diffusion coefficient was 6.0×10^{-6} cm^2/s. These values obtained at the UME also agreed with that at a macroelectrode.

Digital simulation of the CVs was further performed to obtain information on the electrocheical mechanism. The redox formal potentials obtained by digital simulation are presented in Table 1. The oxidation and reduction of T1 were simulated with three reversible one-electron transfers. The experimental and simulated CVs were well fitted at a macroelectrode with 0.5 V/s of scan rate (Figure 2c,d) and with 0.05−5 V/s of scan rate (see Figure S2, S3 in the Supporting Information). The oxidation formal potentials for T1 are $E^0_{1,ox}$ = 1.14 V, $E^0_{2,ox}$ = 1.18 V and $E^0_{3,ox}$ = 1.22 V vs SCE, respectively, using an EEE mechanism with >0.01 cm/s of heterogeneous rate constant. The reduction formal potentials of T1 are $E^0_{1,red}$ = −2.10 V, $E^0_{2,red}$ = −2.16 V and $E^0_{3,red}$ = −2.22 V vs SCE, respectively, using an EEEC mechanism with 1 s^{-1} of homogeneous forward rate constant and >0.005 cm/s of heterogeneous rate constant.

DOI: 10.1021/jacs.5b12184
J. Am. Chem. Soc. 2016, 138, 1947−1954

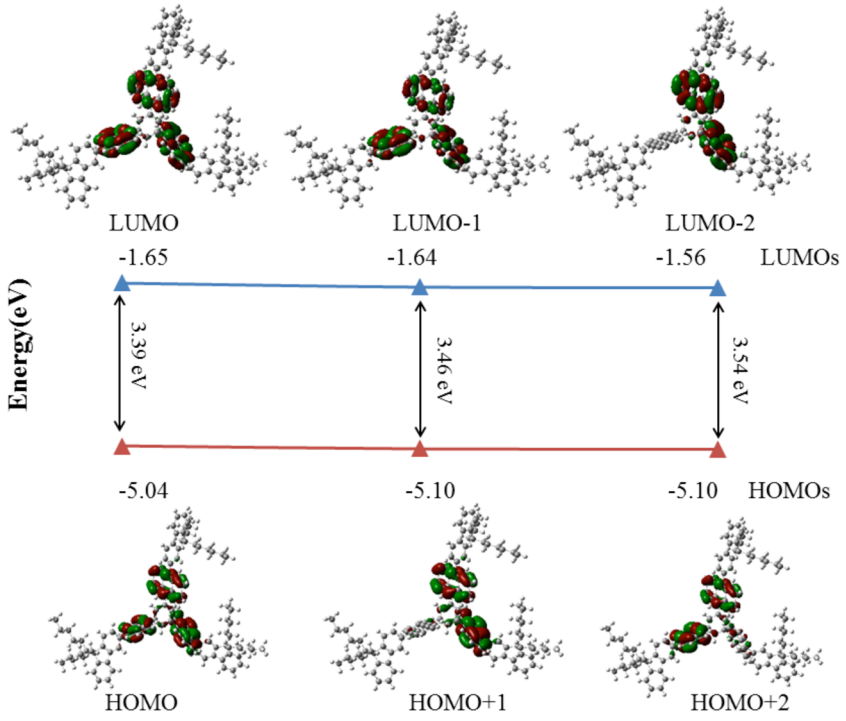

Figure 3. Calculated frontier molecular orbitals of HOMOs and LUMOs for T1 by DFT (B3LYP/6-31G(d)).

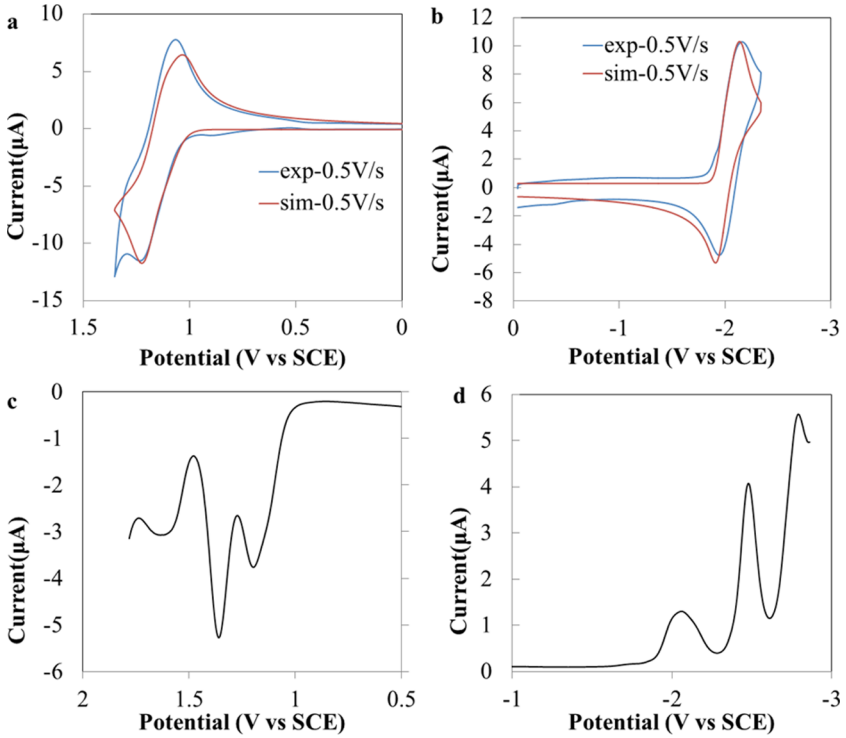

Figure 4. (a) Experimental and simulated oxidation waves of 0.3 mM T2 (EEE, k_1^0 = 0.01 cm/s, k_2^0 = 0.01 cm/s, k_3^0 = 0.1 cm/s. Simulated data: $E^0_{1,ox}$ = 1.11 V, $E^0_{2,ox}$ = 1.16 V, $E^0_{3,ox}$ = 1.18 V; Diffusion coefficient: 6.0× 10^{-6} cm^2/s, uncompensated resistance 1799 Ω, capacitance 1 × 10^{-7} F). (b) Experimental and simulated reduction waves of 0.3 mM T2 (EEEC, k_1^0 = 0.01 cm/s, k_2^0 = 0.01 cm/s, k_3^0 = 0.005 cm/s, k_f = 2 s^{-1}. Simulated data: $E^0_{1,red}$ = −1.98 V, $E^0_{2,red}$ = −2.03 V, $E^0_{3,red}$ = −2.08 V; Diffusion coefficient: 6.0 × 10^{-6} cm^2/s, uncompensated resistance 449 Ω, capacitance 6 × 10^{-7} F); (c) SWV of 0.6 mM T2 for oxidation; (d) SWV of 0.6 mM T2 for reduction; Experimental conditions are same as Figure 2.

It is expected that the theoretical potential differences between the first and second electron transfers is 36 mV if two redox groups are completely uncoupled.[32] Here, $\Delta E_{1,2}$ between the A^+/A and A^{2+}/A^+ and $\Delta E_{2,3}$ between the A^{2+}/A^+ and A^{3+}/A^{2+} are 40 mV for the T1 oxidation while $\Delta E_{1,2}$ between the A^+/A and A^{2+}/A^+ and $\Delta E_{2,3}$ between the A^{2+}/A^+ and A^{3+}/A^{2+} are 60 mV for the T1 reduction. These indicate a weak electronic coupling between the three anthracene groups in the core.[33] These phenomena are consistent with following density functional theory (DFT) calculations.

DOI: 10.1021/jacs.5b12184
J. Am. Chem. Soc. 2016, 138, 1947−1954

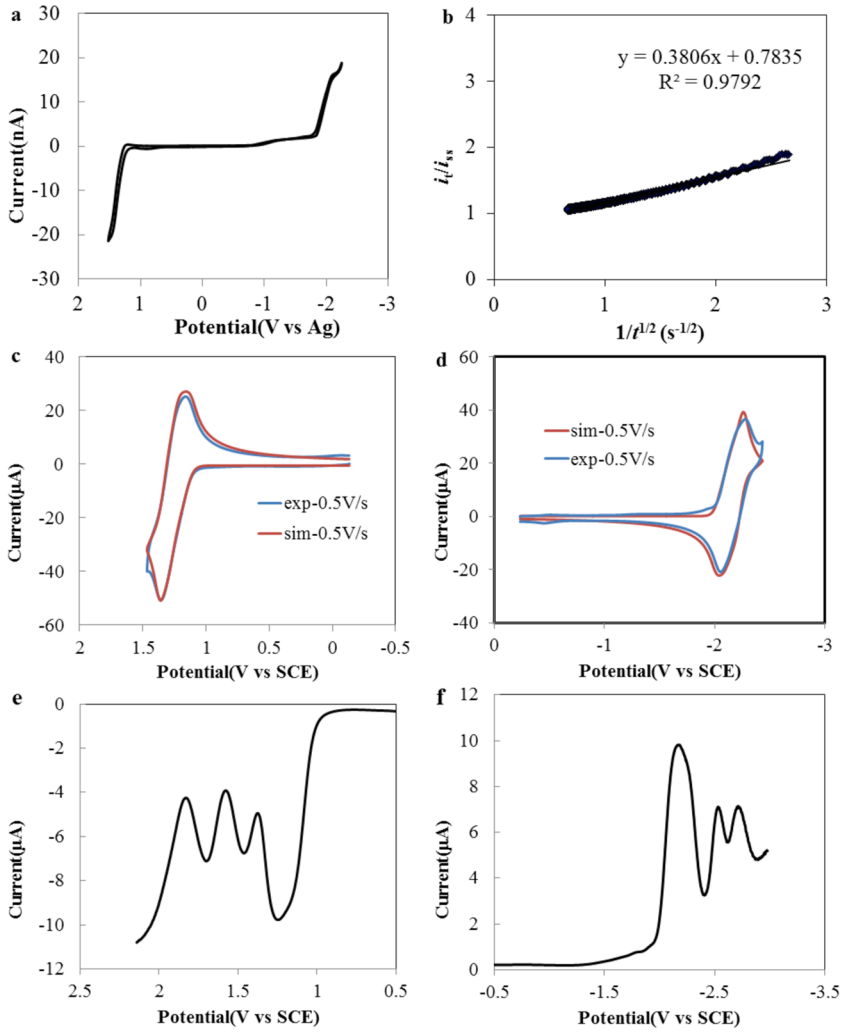

Figure 5. (a) CV of 0.6 mM T3 at gold UME with a scan rate of 5 mV/s. (b) Plot of i_t/i_{ss} vs $t^{-1/2}$ for 0.6 mM T3. (c) Experimental and simulated oxidation waves for 0.7 mM T3 (EEEEEE, $k^0 = 10^4$ cm/s. Simulated data: $E^0_{1,ox} = 1.16$ V, $E^0_{2,ox} = 1.2$ V, $E^0_{3,ox} = 1.24$ V, $E^0_{4,ox} = 1.26$ V, $E^0_{5,ox} = 1.3$ V, $E^0_{6,ox} = 1.32$ V; Diffusion coefficient: 6.0×10^{-6} cm^2/s, uncompensated resistance 617 Ω, capacitance 1×10^{-6} F); (d) Experimental and simulated reduction waves for 0.56 mM T3 (EEEEEE, $k^0 = 10^4$cm/s. Simulated data: $E^0_{1,red} = -2.05$ V, $E^0_{2,red} = -2.09$ V, $E^0_{3,red} = -2.13$ V, $E^0_{4,red} = -2.17$ V, $E^0_{5,red} = -2.21$ V, $E^0_{6,red} = -2.25$ V; Diffusion coefficient: 6.0×10^{-6} cm^2/s, uncompensated resistance 611 Ω, capacitance 2×10^{-7} F); (e) SWV of 0.56 mM T3 for oxidation; (f) SWV of 0.56 mM T3 for reduction. Experimental conditions are same as Figure 2.

The DFT calculations were carried out as described in Computation for T1 by B3LYP/6-31G(d). The calculated HOMO and LUMO energies as well as the HOMO−LUMO gaps for T1 are sketched in Figure 3. Both of the HOMOs and the LUMOs are localized principally on the core. This indicates that the oxidation and reduction are mainly occurring on the core. There is no evidence for electronic delocalization between the core and the attached fluorene arms. It is worth noting that the differences among the energies of HOMO, HOMO−1 and HOMO−2 are small while the energies of LUMO, LUMO+1, and LUMO+2 are almost equal. Additionally, the dihedral angles between each three inflexible anthracene groups and the central benzene are 74.8°, 73.28°, and 114.2°, respectively. This is attributed to the twisted steric effect among three anthracene rings in a 3D room and a weak electronic coupling between the three anthracene groups. All the calculation results are consistent with the small electrochemical potential separation.[34]

In order to obtain information on the arms on the core of T1, the electrochemical scans to more negative and positive potentials were carried out. A second oxidation wave at +1.60 V vs SCE and a second reduction wave at −2.55 V vs SCE were observed in the CVs of T1 (see Figure S4a in the Supporting Information). This is attributed to the addition/removal of electrons on fluorene arms. These were confirmed by DFT calculations (see Figure S5 in the Supporting Information) and square wave voltammetry (Figure 2e,f). In Figure 2e,f, the oxidation current peaks at +1.20 V and +1.60 V vs SCE and the reduction current peaks at −2.20 V and −2.55 V vs SCE appeared, respectively. Furthermore, another three one-electron transfers generated from three fluorene arms are supported by CVs at a UME, in which the steady state current for the second oxidation wave in more positive potentials was the same with that of the first oxidation wave (see Figure S6 in the Supporting Information).

T2. Figure 1b shows CV of T2 at a platinum macroelectrode. One pair of reversible redox waves appears at about +1.19 V vs SCE and at −2.05 V vs SCE for the oxidation and reduction of T2, respectively. To study further the electrochemical mechanism of T2, the digital simulation of the CVs with the experimental CVs at a macroelectrode was performed. The oxidation of T2 was characterized by an EEE mechanism with each reversible one-electron transfer (Figures 4a and Figure S7

DOI: 10.1021/jacs.5b12184
J. Am. Chem. Soc. 2016, 138, 1947−1954

in the Supporting Information). The oxidation formal potentials of T2 are simulated to be $E^0_{1,ox}$ = 1.11 V, $E^0_{2,ox}$ = 1.16 V and $E^0_{3,ox}$ = 1.18 V vs SCE, as shown in Table 1. The reduction of T2 was done by an EEEC mechanism with $E^0_{1,red}$ = −1.98 V, $E^0_{2,red}$ = −2.03 V and $E^0_{2,red}$ = −2.08 V vs SCE (Figure 4b and Figure S8 in the Supporting Information). $\Delta E_{1,2}$ in the formal potential between the A^+/A and A^{2+}/A^+ and $\Delta E_{2,3}$ in the formal potential between the A^{2+}/A^+ and A^{3+}/A^{2+} are 50 mV for the reduction of T2. The $\Delta E_{1,2}$ and $\Delta E_{2,3}$ in the formal potential are 50 mV and 20 mV for the oxidation of T2, respectively. The small potential separations indicate a slightly weak electronic coupling among the three anthracene groups in the core. The frontier molecular orbitals calculated suggest that both of the oxidation and reduction are generated from the core of T2, since both of the LUMOs and the HOMOs are localized principally on the core (Figure S9). The calculated energies are −1.68 eV for LUMO, −1.67 eV for LUMO+1, −1.59 eV for LUMO+2, −5.06 eV for HOMO, −5.12 eV for HOMO−1 and −5.13 eV for HOMO−2, respectively. The LUMOs and HOMOs energies of T2 are slightly lower than that of T1. This trend is consistent with that of the electrochemical formal potential in the CVs.

Both second wave and third wave are observed at more negative and positive potentials (Figure S4b), indicating that T2 can be further oxidized and reduced. The square wave voltammograms (SWV) of T2 clearly show the oxidation current peaks at +1.19 V, + 1.36 V and +1.63 vs SCE, respectively; and the reduction current peaks at −2.05 V, −2.48 V and −2.79 V vs SCE, respectively (Figure 4c,d). The steady-state currents of the second and third oxidation waves are the same with that of the first oxidation waves at UMEs (see Figure S10a in the Supporting Information). Therefore, the second and third oxidation processes of T2 are still three one-electron transfer processes. This is consistent with the result from the CVs at macroelectrode (Figure S10b). DFT of T2 suggests that these oxidation and reduction are carried out on the fluorene arms, since both of the LUMOs and the HOMOs are localized principally on the arms (see Figure S11 in the Supporting Information).

T3. At a macroelectrode, the CV of T3 demonstrates a single reversible oxidation wave at +1.25 V vs SCE and a single reversible reduction at −2.17 V vs SCE (Figure 1c). At a gold UME, the CV of T3 exhibits two nernstian steady-state shapes at half-wave potential of +1.40 vs Ag for oxidation and at half-wave potential of −1.98 V vs Ag for reduction (Figure 5a). From the data of the plot of i_t/i_{ss} vs $t^{-1/2}$ in Figure 5b, the number of electron in the oxidation was found to be 6.18 and the diffusion coefficient of T3 was calculated to be 6.0×10^{-6} cm^2/s. The number of electron for the reduction is deduced to be six from the same of steady-state currents for the oxidation and reduction (Figure 5a). This multiple six-electron transfers were confirmed by digital simulation of the CVs at a macroelectrode with 0.5 V/s (Figure 5c,d) and 0.1−5 V/s (see Figure S12, S13 in the Supporting Information). The observed CVs for oxidation were well reproduced by EEEEEE mechanism, in which the oxidation potentials for T3 are $E^0_{1,ox}$ = 1.16 V, $E^0_{2,ox}$ = 1.20 V, $E^0_{3,ox}$ = 1.24 V, $E^0_{4,ox}$ = 1.26 V, $E^0_{5,ox}$ = 1.30 V, $E^0_{6,ox}$ = 1.32 V vs SCE. Additionally, for the reduction, the potentials are simulated to be $E^0_{1,red}$ = −2.05 V, $E^0_{2,red}$ = −2.09 V, $E^0_{3,red}$ = −2.13 V, $E^0_{4,red}$ = −2.17 V, $E^0_{5,red}$ = −2.21 V, $E^0_{6,red}$ = −2.25 V vs SCE, respectively, assuming an EEEEEE mechanism (Figure 5d, Figure S13). We tried to calculate orbital energy of T3 by DFT, but it is too expensive to obtain the DFT results. According to the results of T1 and T2, it can be deduced that the fluorene arms in T3 may be oxidized at less positive potential and the oxidation waves of the fluorene arms were merged with the oxidation of the anthracenes. For the reduction of T3, the case is the same as for oxidation. Therefore, six-electron transfers of T3 may come from three anthracene groups in the core and three fluorene arms.

For T3, there are second, and third oxidation and reduction peaks at more positive and negative potentials, attributed to the removal and addition of electron on another six fluorene arms (see Figure S4c and Figure S14 in the Supporting Information). It is supported by SWV showing three peaks at +1.25 V, 1.46 V and +1.70 V vs SCE for oxidation, −2.17 V, −2.53 V and −2.72 V vs SCE for reductions, respectively (Figure 5e,f). A higher potential resolution technique is needed to prove such successive electron transfer processes.

For oxidation, $\Delta E_{1,2}$ of T3 (0.21 V) in the peak potential is bigger than $\Delta E_{1,2}$ of T2 (0.17 V); for reduction, $\Delta E_{1,2}$ of T3 (0.36 V) in the peak potential is bigger than $\Delta E_{1,2}$ of T1 (0.33 V). This can be predicted as a Coulombic repulsion between six charged anions. However, $\Delta E_{1,2}$ of T3 (0.21 V) in the peak potential is smaller than $\Delta E_{1,2}$ of T1 (0.40 V) and $\Delta E_{2,3}$ of T3 (0.24 V) is smaller than $\Delta E_{2,3}$ of T2 (0.27 V) for oxidation; $\Delta E_{1,2}$ of T3 (0.36 V) is smaller than $\Delta E_{1,2}$ of T2 (0.43 V) and $\Delta E_{2,3}$ of T3 (0.19 V) is smaller than $\Delta E_{2,3}$ of T2 (0.31 V) for reduction. These may be ascribed to the conformational change of these complex star-shaped compounds during the electron transfer.

Spectroscopy and Electrogenerated Chemiluminescence. The absorption and photoluminescence (PL) emission spectra of T1, T2 and T3 were recorded in MeCN:Bz solution under air-saturated conditions, and shown in Figure 6. Table 2

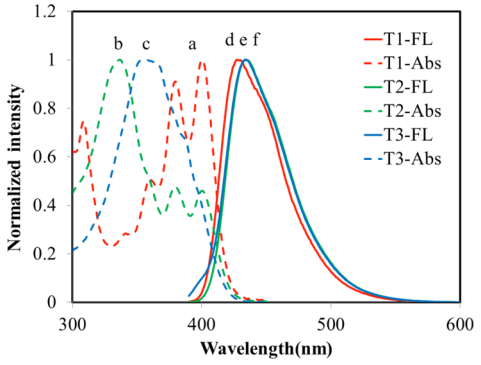

Figure 6. Normalized absorbance spectra (dashed lines) and photoluminescence spectra (solid lines) of T1 (a, d), T2 (b, e), and T3 (c, f). Emission spectra were excited at the maximum absorption wavelength.

Table 2. Photophysical Properties of T1, T2 and T3 in MeCN:Bz (*v*:*v* = 1:1)

dye	λ_{max} (abs) (nm)	λ_{max} (PL) (nm)	E_s [a] (eV)	$-\Delta H_{ann}$ [b] (eV)	λ_{max} (ECL) (nm)	relative Φ_{ECL} [c]
T1	307, 336, 357, 378, 398	427	2.90	3.14	434	0.24
T2	336, 376, 397	434	2.85	2.99	441	0.20
T3	354	434	2.85	3.11	452	0.34

[a] E_s = 1239.81/λ_{max} PL (nm). [b] $-\Delta H_{ann} = E^o_{ox} - E^o_{red} - 0.1$ eV. [c] Relative Φ_{ECL} of DPA is 1.00.

DOI: 10.1021/jacs.5b12184
J. Am. Chem. Soc. 2016, 138, 1947−1954

lists the corresponding spectral results. As seen from Figure 6, the normalized absorbance spectrum of T1 displays typical narrow absorption peaks of fluorene arms being located at 307, 336, and 357 nm and typical narrow absorption features of anthracene at 378 and 398 nm (Figure 6a). T2 exhibits maximum absorptions at 336, 376, and 397 nm (Figure 6b). T1 and T2 exhibit characteristic vibronic features of the isolated fluorene arms and anthracene groups. T3 displays one broad absorption peak at 354 nm (Figure 6c), which is due to the overlap of the $\pi-\pi^*$ transition of the fluorene arms and anthracene groups in the core. T2 and T3 exhibit maximum absorption at 332 and 354 nm, respectively. Compared with T2, T3 has red-shift of 12 nm. This is attributed to the extension of fluorene arms.

The normalized PL spectrum of T1 displays maximum emission at 427 nm (Figure 6d) and that of T2 and T3 exhibit maximum emission at 434 nm (Figure 6e,f). Compared with T1, T2 and T3 have a 7 nm of red shift. This indicates that the core, the arms, and the effective conjugation affect the emissions of these starburst compounds. Importantly, these results suggest that in PL properties, the core mainly dominates, while the arm plays accessory role and the effective conjugation quickly saturates.

ECL can be generated by radical ion annihilation if both of radical cations and anions can undergo energetic electron-transfer reactions. Because of the stability of the radical ions of T1−T3, ion annihilation ECL was collected for T1−T3. The ECL and corresponding CVs were recorded for T1−T3 (see Figure S15 in the Supporting Information), indicating that the radical ions of T1−T3 are stable and ECL emissions are generated. Figure 7 shows the ECL spectra of T1−T3 in ion

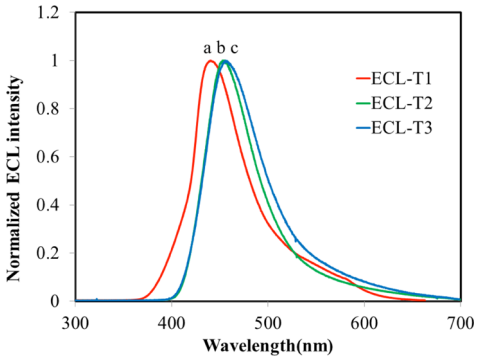

Figure 7. ECL spectra of T1 (red, a), T2 (green, b) and T3 (blue, c) generated by ion annihilation with a pulse width of 0.1 s from about 80 mV past oxidation and reduction potentials. Experimental conditions are same as Figure 2.

annihilation obtained by pulsing technique. The ECL data are listed in Table 2. The compounds all produce blue ECL emissions and the maximum ECL emissions of T1, T2 and T3 are 434 nm, 441 and 452 nm, respectively. A slight red-shift in the maximum ECL wavelength and a broadness in the ECL spectra were observed for T1, T2 and T3, compared with that of PL emissions (see in Figure S16 in the Supporting Information). The red-shift and the broadness in the ECL spectra can be ascribed to the different conditions. First, the different concentrations were used in the PL measurement (μM level) and ECL measurement (mM level). Second, the difference instruments with different resolutions and slit widths were used for PL and ECL measurements.[22,35] Although the ECL spectra of T1−T3 had different shapes in long wavelength region compared with their PL spectra, the ECL spectra did not show additional peaks from electrolyzed byproduct emission[36] or excimer emission.[37]

The ECL efficiencies (Φ_{ECL}) were determined by choosing diphenylanthracene (DPA) as standard in MeCN:Bz (v:v = 1:1). With respect to DPA, the relative ECL efficiency of T1−T3 was found to be 0.24, 0.20, and 0.34 respectively, as listed in Table 2.

The ECL mechanism of T1, T2 and T3 was demonstrated by comparing the annihilation energy ($-\Delta H_{ann}$) with the energy of the excited singlet state (E_s). The E_s was calculated to be 2.90 eV for T1, 2.85 eV for T2 and 2.85 eV for T3, respectively, using the equation E_s (eV) = 1239.81/λ_{max} (nm, PL). The $-\Delta H_{ann}$ was calculated to be 3.14 eV for T1, 2.99 eV for T2 and 3.11 eV for T3, respectively, by using the equation $-\Delta H_{ann} = E^0_{ox} - E^0_{red} - 0.1$ eV. It is well-known that if the energy of the $-\Delta H_{ann}$ is larger than that the E_s, ^{1}R* can be directly generated and the system is the energy-sufficient system, i.e., the S-route is identified for the ECL reaction.[38] Here, $-\Delta H_{ann}$ calculated from the electrochemical data is bigger than the E_s. Therefore, the ECL process of this system is identified as the S-route.

CONCLUSION

The electrochemistry and ECL of three 1,3,5-tri(anthracen-10-yl)-benzene-centered starburst oligofluorenes were studied. T1 and T2 show three reversible, one-electron transfers and T3 shows six reversible, one-electron transfers for the oxidation and reduction processes. The multiple electron transfers are confirmed by chronoamperometry at an ultramicroelectrode, digital simulations and DFT calculations. Strong blue ECL emission can be generated under ion annihilation condition from T1−T3, assigned as S-route, and the ECL spectrum generated by ion annihilation is similar to the photoluminescence emission of these compounds. These results demonstrate that T1−T3 can be used as promising candidates for future ECL materials because of their unique electrochemical and optical properties.

ASSOCIATED CONTENT

Supporting Information

The Supporting Information is available free of charge on the ACS Publications website at DOI: 10.1021/jacs.5b12184.

Experimental and simulated CVs, calculated frontier molecular orbitals of HOMOs and LUMOs, PL spectra and ECL data. (PDF)

AUTHOR INFORMATION

Corresponding Authors

*wanglei@mail.hust.edu.cn

*ajbard@cm.utexas.edu

Notes

The authors declare no competing financial interest.

ACKNOWLEDGMENTS

This work was financially supported by the National Science Foundation (CHE- 1405248) and the Welch Foundation (F-0021). Dr. Honglan Qi thanks The National Science Foundation of China (Nos. 21522504, 21375084, 21475082) and the 111 project (B14041) for support.

DOI: 10.1021/jacs.5b12184
J. Am. Chem. Soc. 2016, 138, 1947−1954

REFERENCES

(1) Molina, A.; Serna, C.; Li, Q.; Laborda, E.; Batchelor-McAuley, C.; Compton, R. G. *J. Phys. Chem. C* **2012**, *116*, 11470−11479.
(2) Flanagan, J. B.; Margel, S.; Bard, A. J.; Anson, F. C. *J. Am. Chem. Soc.* **1978**, *100*, 4248−4253.
(3) Nepomnyashchii, A. B.; Broring, M.; Ahrens, J.; Bard, A. J. *J. Am. Chem. Soc.* **2011**, *133*, 8633−8645.
(4) Hou, J.-M.; Gao, X.-X. *Gaodeng Xuexiao Huaxue Xuebao* **1994**, *15*, 1136−1139.
(5) Fillaut, J.-L.; Astruc, D.; Linares, J. *Angew. Chem., Int. Ed. Engl.* **1995**, *33*, 2460−2462.
(6) Hartmann, H.; Berger, S.; Winter, R.; Fiedler, J.; Kaim, W. *Inorg. Chem.* **2000**, *39*, 4977−4980.
(7) Xie, Q.; Perez-Cordero, E.; Echegoyen, L. *J. Am. Chem. Soc.* **1992**, *114*, 3978−3980.
(8) Qi, H.; Chang, J.; Abdelwahed, S. H.; Thakur, K.; Rathore, R.; Bard, A. J. *J. Am. Chem. Soc.* **2012**, *134*, 16265−16274.
(9) Jarosz, T.; Lapkowski, M.; Ledwon, P. *Macromol. Rapid Commun.* **2014**, *35*, 1006−1032.
(10) Kanibolotsky, A. L.; Perepichka, I. F.; Skabara, P. J. *Chem. Soc. Rev.* **2010**, *39*, 2695−2728.
(11) Hadjichristidis, N.; Pitsikalis, M.; Pispas, S.; Iatrou, H. *Chem. Rev.* **2001**, *101*, 3747−3792.
(12) Omer, K. M.; Kanibolotsky, A. L.; Skabara, P. J.; Perepichka, I. F.; Bard, A. J. *J. Phys. Chem. B* **2007**, *111*, 6612−6619.
(13) Kanibolotsky, A. L.; Berridge, R.; Skabara, P. J.; Perepichka, I. F.; Bradley, D.D. C.; Koeberg, M. *J. Am. Chem. Soc.* **2004**, *126*, 13695−13702.
(14) Mohsan, Z.; Kanibolotsky, A. L.; Stewart, A. J.; Inigo, A. R.; Dennany, L.; Skabara, P. J. *J. Mater. Chem. C* **2015**, *3*, 1166−1171.
(15) Katsis, D.; Geng, Y. H.; Ou, J. J.; Culligan, S. W.; Trajkovska, A.; Chen, S. H.; Rothberg, L. J. *Chem. Mater.* **2002**, *14*, 1332−1339.
(16) Zhou, X.-H.; Yan, J.-C.; Pei, J. *Org. Lett.* **2003**, *5*, 3543−3546.
(17) Lin, W.-J.; Chen, W.-C.; Wu, W.-C.; Niu, Y.-H.; Jen, A. K.-Y. *Macromolecules* **2004**, *37*, 2335−2341.
(18) Lai, W.-Y.; Zhu, R.; Fan, Q.-L.; Hou, L.-T.; Cao, Y.; Huang, W. *Macromolecules* **2006**, *39*, 3707−3709.
(19) Liu, C.; Li, Y.; Zhang, Y.; Yang, C.; Wu, H.; Qin, J.; Cao, Y. *Chem. - Eur. J.* **2012**, *18*, 6928−6934.
(20) Liu, C.; Li, Y.; Li, Y.; Yang, C.; Wu, H.; Qin, J.; Cao, Y. *Chem. Mater.* **2013**, *25*, 3320−3327.
(21) Liu, C.; Fu, Q.; Zou, Y.; Yang, C.; Ma, D.; Qin, J. *Chem. Mater.* **2014**, *26*, 3074−3083.
(22) Suk, J.; Natarajan, P.; Moorthy, J. N.; Bard, A. J. *J. Am. Chem. Soc.* **2012**, *134*, 3451−3460.
(23) Liu, T.-A.; Prabhakar, C.; Yu, J.-Y.; Chen, C.-h.; Huang, H.-H.; Yang, J.-S. *Macromolecules* **2012**, *45*, 4529−4539.
(24) Li, B.; Li, J.; Fu, Y.; Bo, Z. *J. Am. Chem. Soc.* **2004**, *126*, 3430−3431.
(25) Ren, S.; Zeng, D.; Zhong, H.; Wang, Y.; Qian, S.; Fang, Q. *J. Phys. Chem. B* **2010**, *114*, 10374−10383.
(26) Tan, L. L.; Chen, H. Y.; Hao, L. F.; Shen, Y.; Xiao, L. M.; Liu, J. M.; Kuang, D. B.; Su, C. Y. *Phys. Chem. Chem. Phys.* **2013**, *15*, 11909−11917.
(27) Sartin, M. M.; Shu, C.; Bard, A. J. *J. Am. Chem. Soc.* **2008**, *130*, 5354−5360.
(28) Hadjichristidis, N.; Pitsikalis, M.; Pispas, S.; Iatrou, H. *Chem. Rev.* **2001**, *101*, 3747−3792.
(29) Huang, H.; Fu, Q.; Zhuang, S.; Liu, Y.; Wang, L.; Chen, J.; Ma, D.; Yang, C. *J. Phys. Chem. C* **2011**, *115*, 4872−4878.
(30) Qi, H.; Chen, Y.-H.; Cheng, C.-H.; Bard, A. J. *J. Am. Chem. Soc.* **2013**, *135*, 9041−9049.
(31) Denuault, G.; Mirkin, M. V.; Bard, A. J. *J. Electroanal. Chem. Interfacial Electrochem.* **1991**, *308*, 27−38.
(32) Ammar, F.; Saveant, J. M. *J. Electroanal. Chem. Interfacial Electrochem.* **1973**, *47*, 215−221.
(33) Itaya, K.; Bard, A. J.; Szwarc, M. *Z. Phys. Chem.* **1978**, *112*, 1−9.
(34) Boulas, P. L.; Gomez-Kaifer, M.; Echegoyen, L. *Angew. Chem., Int. Ed.* **1998**, *37*, 216−247.
(35) Sartin, M. M.; Camerel, F.; Ziessel, R.; Bard, A. J. *J. Phys. Chem. C* **2008**, *112*, 10833−10841.
(36) Qi, H.; Teesdale, J. J.; Pupillo, R. C.; Rosenthal, J.; Bard, A. J. *J. Am. Chem. Soc.* **2013**, *135*, 13558−13566.
(37) Suk, J.; Wu, Z.; Wang, L.; Bard, A. J. *J. Am. Chem. Soc.* **2011**, *133*, 14675−14685.
(38) Miao, W. *Chem. Rev.* **2008**, *108*, 2506−2553.

DOI: 10.1021/jacs.5b12184
J. Am. Chem. Soc. 2016, 138, 1947−1954